Available online at www.sciencedirect.com
ScienceDirect
Ceramics International 37 (2011) 3109–3116
CERAMICS INTERNATIONAL
www.elsevier.com/locate/ceramint

Thermodynamic simulation models for predicting Al_2O_3–MgO castable chemical corrosion

A.P. Luz [a,*], M.A.L. Braulio [a], A.G. Tomba Martinez [b], V.C. Pandolfelli [a]

[a] Federal University of São Carlos, Materials Engineering Department, Rod. Washington Luiz, km 235, São Carlos – SP, C.P. 676, CEP 13565-905, Brazil
[b] Materials Science and Technology Research Institute (INTEMA), Ceramics Division, Av. Juan B. Justo 4302, 7600 Mar del Plata, Argentina

Received 5 May 2011; accepted 12 May 2011
Available online 18 May 2011

Abstract

The chemical corrosion of two Al_2O_3–MgO castables (containing distinct binder sources: hydratable alumina or calcium aluminate cement) were evaluated in this work via thermodynamic calculations. Two simulation models were proposed according to the following procedures: (1) firstly the matrix and later the aggregates of the castables were placed, separately, in contact with an industrial basic slag, and (2) the overall chemical composition of the design castables was directly reacted with the molten slag. The theoretical results were further compared with experimental data collected after corrosion cup tests. Although the thermodynamic evaluation of the overall castable compositions was able to identify the phase transformations correctly, a two-step analysis of the matrix components and aggregates particles seems to be the best alternative to evaluate the binder source effect on the corrosion performance of the two Al_2O_3–MgO refractory materials.

Keywords: C. Corrosion; Spinel containing castables; Thermodynamic simulation; Spinel

1. Introduction

Corrosion of refractory castables is a complex phenomenon which has been extensively studied [1–6]. Depending on the system, refractory wear may comprise chemical (corrosion) and physical or mechanical (erosion) processes. Chemical corrosion takes place as the evaluated system attempts to attain the equilibrium when the molten liquid is not saturated with a refractory component. Therefore, the thermodynamic equilibrium will only be achieved by the dissolution of that refractory component up to the liquid saturation [5].

Although the bulk slag has an important influence on the corrosion process, the composition of the local molten slag penetrating the refractory is also critical. The local liquid may present some changes due to the dissolution of the binder and grains or the incorporation of species as for the spinel (which can accommodate Al_2O_3, FeO or MnO in its structure) [1]. Moreover, iron and manganese ions, which diffuse faster than others, may penetrate farther into the refractory. Therefore, the corrosion rate is a function of many variables including temperature, refractory/liquid/interface composition, and liquid density, viscosity, diffusivity and stirring rate [5–8].

Spinel containing castables are heterogeneous materials comprised by coarse alumina aggregates and a finer, more porous intergranular matrix. The higher porosity and fine texture of the matrix make it more reactive than the aggregates. Consequently, castable wear also depends on the microstructure of the refractory and its physicochemical properties, including type of bond and grain size distribution [2,4,9].

The reaction between refractory and molten slags should be described taking into account both the thermodynamic (equilibrium conditions) and the kinetic aspects (reaction rates). Thermodynamic calculations are particularly suitable to understand the corrosion phenomena. By analyzing the reactions at equilibrium, better knowledge of the corrosion mechanisms can be attained by improving industrial performance and reducing the need of experimental tests [4].

Recently, some work has focused on developing simulation models to evaluate refractory corrosion behavior [2,3,9]. Although the proposed procedures provide very useful information, they do not take into account the slag saturation and the changes of its chemical composition during the reaction

* Corresponding author. Tel.: +55 16 33518253; fax: +55 16 33615404.
E-mail address: anapaula.light@gmail.com (A.P. Luz).

0272-8842/$36.00
doi:10.1016/j.ceramint.2011.05.049

with the refractory. Thus, in a previous study a new modeling approach was suggested by the present authors [10], when successive calculations, simulating the liquid penetration and its compositional changes, were carried out. According to that article, the predictions attained by the thermodynamic calculations for the spinel containing castable corrosion behavior were in agreement with the experimental tests, but it was also highlighted that some improvements (such as previous evaluation of the molten slag interaction with the matrix compounds and later with the aggregates of the castables) could still be implemented.

Considering these aspects, this work addresses the investigation of a novel thermodynamic simulation procedure, where firstly the matrix and later the aggregates are taken into account during contact between an industrial steel ladle basic slag with two different Al_2O_3–MgO castable compositions. Additionally, the collected results attained by this procedure were compared with the data of simulations involving the interaction between the liquid slag and the overall chemical compositions of the refractories and also with experimental tests (corrosion cup-tests) in order to evaluate the advantages and drawbacks of each calculation procedure.

2. Experimental and thermodynamic calculations

For the two designed vibratable castables (Alfred particle packing model, $q = 0.26$ [11]) coarse tabular alumina was added as aggregates ($d \leq 6$ mm, Almatis, USA) and dead-burnt magnesia ($d < 45$ μm, 95 wt% of MgO, $CaO/SiO_2 = 0.37$, Magnesita Refratários S.A., Brazil), silica fume (971U, Elkem, Norway), reactive alumina (CL370, Almatis, USA) and fine tabular alumina ($d < 200$ μm, Almatis, USA) comprised the matrix of these compositions. Moreover, calcium aluminate cement – *CAC* – (Secar 71, Kerneos, France) or hydratable alumina – *HA* – (AlphaBond 300, Almatis, USA) were selected as binders and their influence on the corrosion behavior were investigated. Table 1 shows their overall compositions.

During the processing step, 0.2 wt% of a polycarboxylate-based dispersant was added to the castable suspensions (Bayer, Germany) in order to ensure suitable dispersion of the fine particles. Additionally, 3.9 and 5.3 wt% of distilled water was required for the IS-6C1S and IS-6H1S mixing, respectively. The prismatic samples used in the corrosion tests (150 mm × 25 mm × 25 mm) were molded, cured at 50 °C for 24 h, dried at 110 °C for 24 h and pre-fired for 5 h at 600 °C. In order to ensure the formation of in situ spinel and calcium hexaluminate (CA_6) in the castable microstructure [12,13], the prepared samples were also thermally treated at 1500 °C for 5 h.

Before the corrosion tests, small cups were drilled into the fired samples (central inner diameter of 10 mm and 10 mm deep), which were filled with a mixture of 90 wt% of the slag (Table 2) and 10 wt% of iron oxide. The corrosion cup tests were conducted in a vertical tube furnace in a controlled oxidizing atmosphere (oxygen partial pressure = 0.21 atm) (HTRV 100-250/18 GERO) at 1550 °C for 2 h. The corroded samples were also cut and their cross sections were polished for scanning electron microscopy evaluation (JEOL JSM – 5900 LV, The Netherlands).

Thermodynamic simulations were carried out using Fact-Sage [version 6.2, Thermfact/CRCT (Montreal) and GTT-Technologies (Aachen)], which comprises a series of modules that access and cross link thermodynamic databases and allow various calculations. For this study, the databases used were Fact53, SGTE and FToxid, and the Equilib and Viscosity modules were selected for the chosen simulations.

Two calculation procedures were developed by the present authors and compared considering the liquid composition changes during the contact between the refractory–slag at high temperatures. According to a first proposed model [10], 100 g of each designed castable (in this case, only the overall compositions was evaluated – Table 1) and 100 g of a slag composition (comprised of a mixture of 90 wt% of an industrial secondary metallurgy slag – Table 2 – and 10 wt% of Fe_2O_3) were considered in the first reaction stage between these two materials. All calculations were made for a constant temperature of 1550 °C and pressure of 1 atm. After the first reaction step, the resulting liquid slag (S_1) was again put in contact with the same amount (100 g) of the original castable composition used before and a further thermodynamic calculation was carried out. This procedure was constantly repeated until the calculated amount of the main solid phases (after all the possible reactions) attained a constant value. After that, the changes in the amount of the phases (predicted by the thermodynamic simulations) formed during the interaction of the liquid with the castables were compared with those attained in experimental corrosion cup-tests.

Nevertheless, it is well known that the matrix portion of the castables (comprised by the binder and other components with finer average particle size, $d < 100$ μm) is very reactive and can be easily incorporated by the slag. Thus, a further route to analyze the castable corrosion consists of the following simulation steps: (1) the contact between the slag and the matrix and after the liquid saturation, (2) the interaction between the resulting slag and the aggregates. In this case, the same procedure described before were applied, where initially

Table 1
General information of the castables compositions.

	Designed compositions	IS-6C1S	IS-6H1S
Raw materials	Tabular ($d < 3$ mm) and reactive alumina ($d_{50} = 4$ μm)	87	87
	Dead-burnt magnesia ($d < 45$ μm)	6	6
	Calcium aluminate cement	6	–
	Hydratable alumina	–	6
	Silica fume	1	1

Table 2
Chemical composition of the industrial secondary metallurgy slag.

Composition	Al_2O_3	MgO	CaO	SiO_2	MnO	Fe_2O_3
Wt%	29.6	3.1	44.9	5.3	2.2	4.9

100 g of slag and 100 g of the castable matrix were reacted and the resulting liquid of each step was successively put in contact with the original matrix, until the slag saturation was reached. After that, 100 g of the resulting slag (liquid saturated with the matrix components) were used in the calculations involving 100 g of the aggregates.

Additionally, in order to define the matrix composition for the thermodynamic simulations (Table 3), not only the amount of the initial raw materials of the designed castables were considered, but also the results attained from quantitative X-ray diffraction (XRD) and scanning electron microscopy (MEV-EDS) evaluations of the fired samples, were used.

Due to the MgO and Al_2O_3 reaction (giving rise to the in situ $MgAl_2O_4$ formation) and the CA_6 generation in the matrix and at the edges of the Al_2O_3 grains after thermal treatment at 1500 °C, these new phases were added to the matrix simulation in order to be closer to the conditions faced by the castables during the experimental tests.

3. Results and discussion

Fig. 1 presents the phase evolution for each castable system at different steps of calculation, considering the first simulation approach, when the overall refractory composition is evaluated.

After the initial contact between the castable and slag, new phases are expected to be formed at the interface area indicating that corrosion is carried out by the dissolution of the original solid and precipitation of CA_2, CA_6 and spinel. Therefore, a final layered microstructure should be attained as a consequence of the liquid saturation by the castable components, resulting in the formation of new phases as the interaction slag-castable takes place.

At the right corner of Fig. 1 is shown the phase content of the fired castable composition attained by thermodynamic simulation, disregarding minor components (i.e., mullite predicted in the IS-6H1S material) and liquid phases, as they would be incorporated by the slag during the chemical corrosion process. As the reaction progress between the liquid (SLAG) and the designed castables, the liquid composition changes up to its saturation and, after that, the refractories should not be further chemically attacked.

The reaction mechanisms and a detailed comparison of the theoretical results with the experimental ones for the corrosion behavior of spinel containing castables are presented and discussed in previous papers by the present authors [10,14].

Table 3
Matrix and aggregates compositions considered for the thermodynamic simulations.

Wt%	Matrix ($d < 100$ μm)		Aggregates ($d > 100$ μm)	
	IS-6C1S	IS-6H1S	IS-6C1S	IS-6H1S
Al_2O_3	12.81	38.30	89.40	100.00
CA_6	20.50	–	10.60	–
$MgAl_2O_4$	61.99	58.90	–	–
CaO	1.80	–	–	–
SiO_2	2.80	2.80	–	–

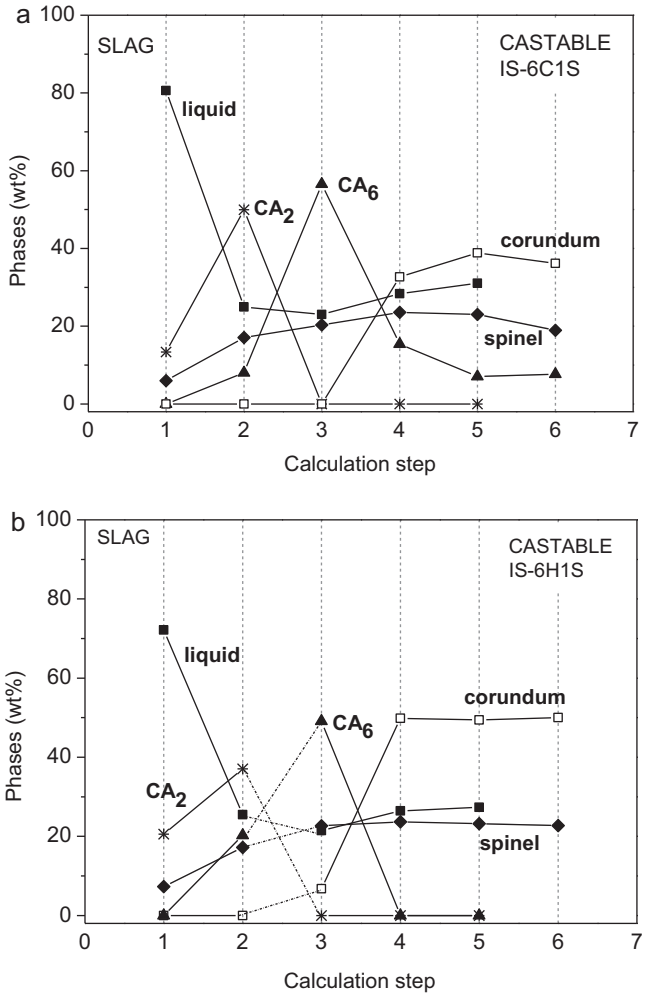

Fig. 1. Phase evolution predicted by the thermodynamic simulations for the contact involving an industrial slag and the overall composition of the spinel containing castables (a) IS-6C1S and (b) IS-6H1S [10].

The following phase transformations are predicted by the calculations with the advance of the slag contact with the IS-6C1S castable:

$$\text{slag} \rightarrow CA_2 + \text{spinel} \rightarrow CA_2 + \text{spinel} + CA_6 \rightarrow CA_6 + \text{spinel} \rightarrow \text{corundum} + \text{spinel} + CA_6 \rightarrow \text{castable}$$

According to the chosen simulation modeling, the corrosion behavior of the IS-6H1S castable (which comprises hydratable alumina instead of calcium aluminate cement) did not show remarkable differences when compared to the IS-6C1S one (Fig. 1). It was observed that the amount of liquid phase in IS-6H1S is lower due to the absence of calcium aluminate cement. Moreover, its initial CA_2 content, after the first contact with the slag (*step 1*, Fig. 1b) is higher and, consequently, the predicted amount of Al_2O_3 and CaO in the liquid phase is slightly lower after the first reaction.

It must also be highlighted that after the initial slag–refractory contact, all the alumina from the castables is dissolved into the liquid (Fig. 1, corundum content is zero at *step 1*). However, as the slag keeps interacting with the

Table 4
Chemical features of the spinel containing castable samples, compared to the attained corrosion results.

Compositions	Chemical features			Corrosion results
	Al_2O_3 content (matrix)	CA_6 content (matrix)	Liquid phase	Penetration
IS-6C1S	Low	High	Yes	High
IS-6H1S	High	Absent	Yes	Low

refractory, corundum might be present due to the saturation of the slag and no more dissolution of this phase is expected to occur. The corundum phase was detected in an earlier step in the IS-6H1S castable and this result is associated with the higher supply of Al_2O_3 in this system. Therefore, based on these data, the IS-6H1S castable should have the highest corrosion resistance, as the thermodynamic equilibrium would have been attained earlier.

The similarities of the amount of the predicted phases for the evaluated castables (presented in Fig. 1) are associated with the assumptions of the model used to calculate the slag–refractory interaction. For example, this procedure disregards important aspects such as the location of the phases in the refractory microstructure (calcium aluminate phase distribution and the content of calcia, alumina and spinel in the castable matrix), the particle size differences between the aggregates and the matrix, and some physical properties of the castable (open porosity and permeability) which also affect the corrosion behavior.

As presented in Table 4, although the thermodynamic predictions for the corrosion behavior are in agreement with the experimental data (IS-6H1S presented the best performance with lower slag penetration), the calculation procedure can still be improved. Considering the XRD and SEM analyses of the fired samples before corrosion tests, it was observed that for the IS-6C1S composition (which was bonded with calcium aluminate cement) CA_6 were formed and located in the matrix region and as a thin layer at the edges of the tabular alumina aggregates (Fig. 2).

This CA_6 formed in situ at the edges of the coarse alumina grains leads to densification, protecting the refractory by slowing down the infiltration [5,15]. Therefore, the presence of this phase should be considered as one of the initial inputs for the calculations.

Additionally, it is well known that the finer matrix can be readily dissolved, modifying the slag composition and affecting further reactions. Considering these aspects, a novel calculation modeling was proposed, where the industrial slag was firstly only placed in contact with the matrix components (Table 3). Afterwards, the resulting saturated liquid also reacted with the alumina aggregates in order to detect whether a slag attack could still take place, giving rise to new phase transformations. Because the kinetic features of the phase transformations are not taken into consideration in the thermodynamic analysis, the procedure of splitting the matrix and aggregate portions might allow a better description of the phase changes during the corrosion process.

Fig. 3 presents the thermodynamic results for the previous interaction of the liquid slag with the matrix compounds and later with the aggregates of the designed spinel containing castables. Due to the earlier Al_2O_3 slag saturation during corrosion of the IS-6H1S matrix composition, no further attack of the aggregates was predicted by the calculations and, therefore, these results are not presented in Fig. 3.

When the molten slag initially contacts the solid, because the slag is not in equilibrium with the matrix components, solution and interdiffusion of different components is carried out, resulting in a compositional gradient which can further lead to the formation of phases such as $MgAl_2O_{4(ss)}$, CA_2 and CA_6. According to the novel calculation procedure, some differences of the castable corrosion behavior are readily identified in Fig. 3a and b.

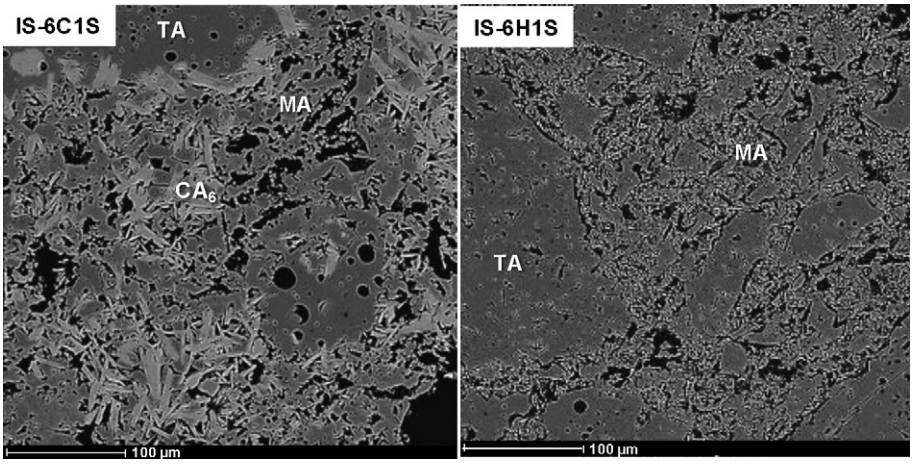

Fig. 2. Castable microstructures after firing at 1500 °C for 5 h (before corrosion cup-tests). TA: tabular alumina, MA: spinel, CA_6: calcium hexaluminate [12].

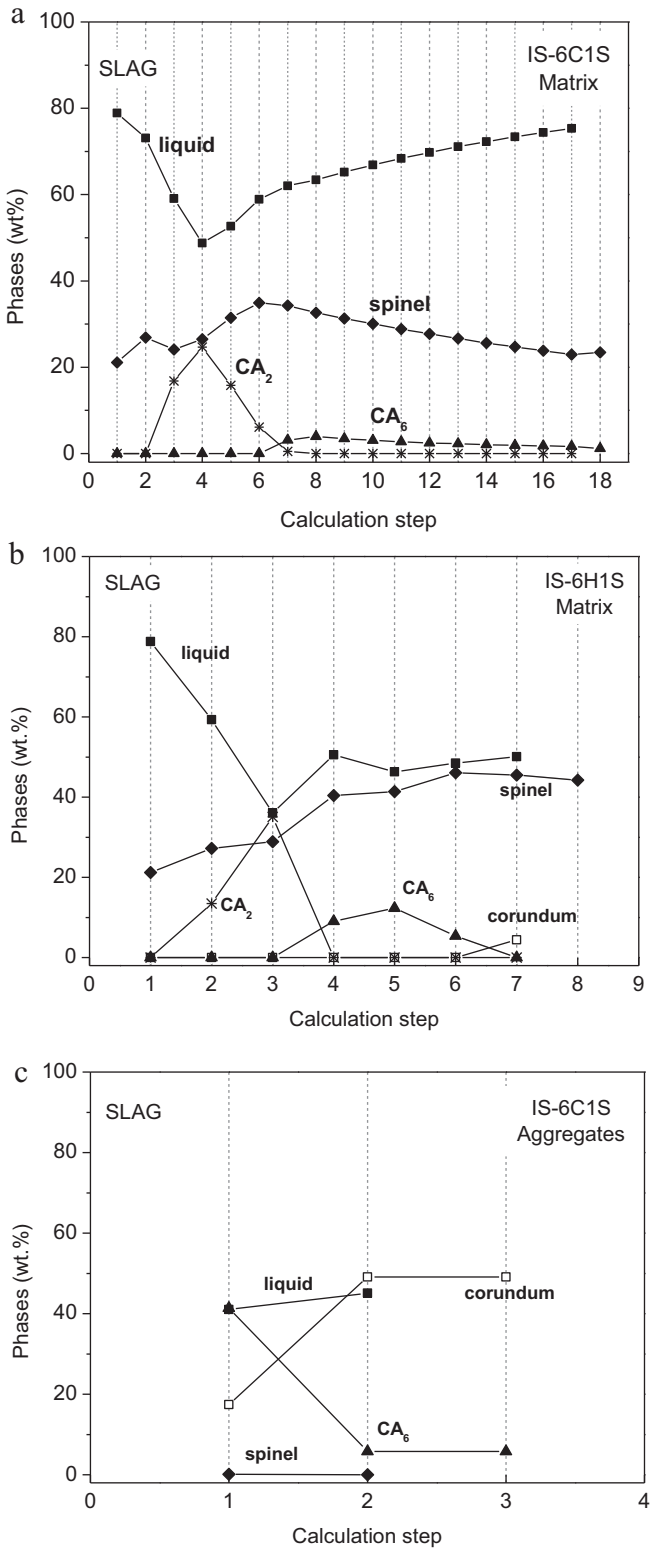

Fig. 3. Phase evolution predicted by the thermodynamic simulations for the contact involving slag–matrix (a) IS-6C1S, (b) IS-6H1S, and slag–aggregates (c) IS-6C1S.

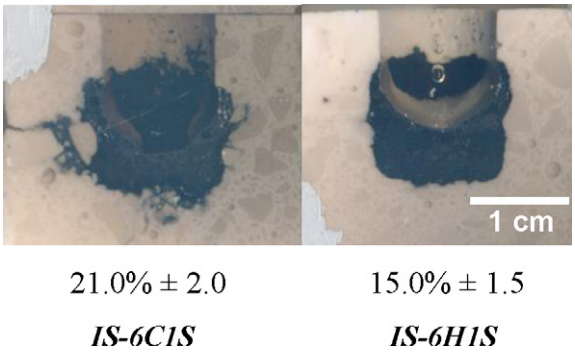

Fig. 4. Cross sections and penetration area (%) of the corroded samples [14].

CaO/CA_6 (derived from the addition of calcium aluminate cement) and the limited amount of Al_2O_3 in the IS-6C1S matrix resulted in a more reactive system and various calculation steps (a total of 17) are necessary to reach the liquid saturation. This result supports the fact that the cement containing composition should be more attacked by the slag, as observed in the experimental tests (Fig. 4), which led to greater amounts of liquid phase (Fig. 3a).

The precipitation of spinel, CA_2 and CA_6 from the liquid is related to the mobility of diffusing species in the slag. According to some work [8,15], the diffusion coefficients of cations are generally believed to take place in the following order: $D_{Fe} > D_M$ (M = Ca, Mg, Mn) $> D_{Al} \gg D_{Si}$.

Therefore, the formation of spinel and calcium aluminates at the slag–matrix interface is favored because Ca^{2+}, Mg^{+} and Al^{3+} can move faster than silicon ions and mainly react with Al_2O_3 to form the corresponding products [1,7,8]. The spinel should also contain Fe_xO and MnO into solid solution, and their concentration can change depending on the location of this phase. For example, the spinel nearer the castable interface should contain more Al_2O_3 and less Fe_xO, MnO and MgO than the one near the bulk slag [8], which indicates that the interdiffusion of the ions affects the spinel formation.

The saturation solubility of Al_2O_3 in the slag has a critical influence on the dissolution process of the studied castables. CA_2 and CA_6 formation is limited due to the lower alumina content in the IS-6C1S matrix (Fig. 3a), however the contact of the resulting slag with the tabular alumina aggregates will lead to further CA_6 generation (Fig. 3c, *step 1*).

SEM images of the infiltrated zones (matrix–liquid region) and of the reacted interface between slag–aggregates are shown in Fig. 5.

The presence of continuous and well defined layers of calcium aluminates at the edge of the tabular alumina aggregates were observed for the IS-6C1S samples. Additionally, the crystal morphologies of the formed phases indicate their precipitation from a liquid source. Spinel and calcium aluminates phases were located between the matrix–slag interface for both compositions containing iron and manganese in their solid solution. In the area closer to the slag, FeO_x and MnO concentration were higher than for deeper refractory regions. Moreover, CA was also observed, but its morphology could not be clearly defined. The presence of CA_6 grains, cubic-shaped spinels and the formation of a layer of CA_2 were detected at the slag–aggregate interface, showing good agreement with the thermodynamic predictions.

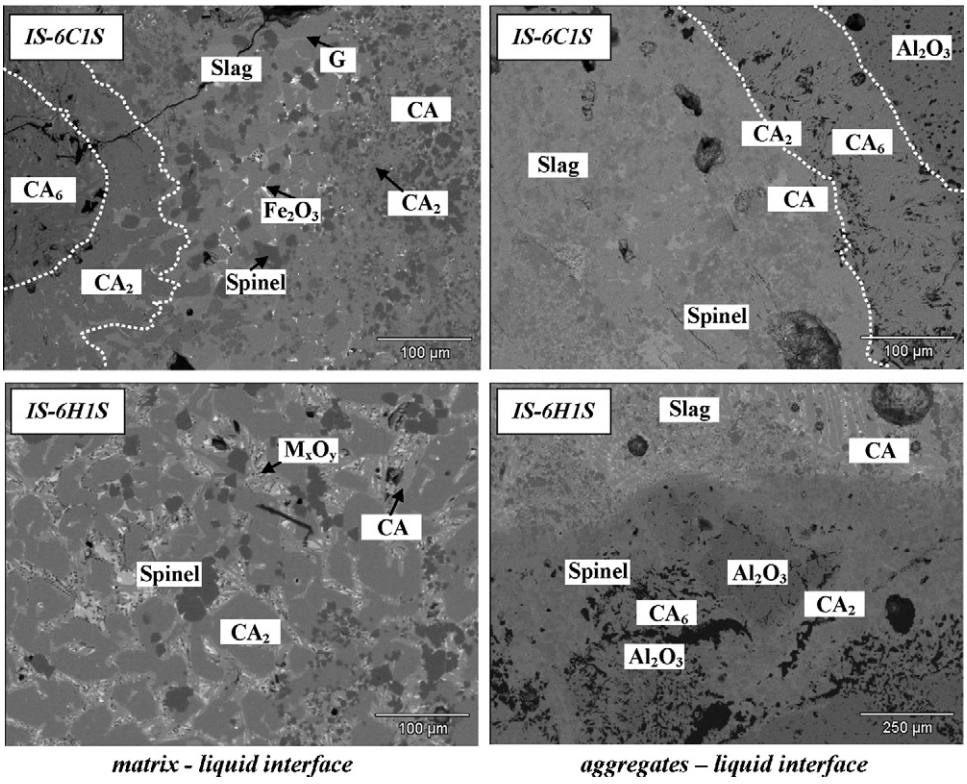

Fig. 5. Corroded regions of the two Al_2O_3–MgO castable compositions. G: gehlenite ($2CaO{\cdot}Al_2O_3{\cdot}SiO_2$); Spinel ($MgAl_2O_4$); CA ($CaO{\cdot}Al_2O_3$); CA_2 ($CaO{\cdot}2Al_2O_3$); CA_6 ($CaO{\cdot}6Al_2O_3$) and M_xO_y ($MgO + MnO + Fe_2O_3$).

As suggested by some authors [7,14], an important aspect that can spoil the corrosion resistance of this sort of refractory is the large differences in the molar volume between CA_6 and Al_2O_3, which can result in the interface disintegration, allowing the molten slag to penetrate into the bulk specimen preferably through the Al_2O_3 grain boundaries. IS-6C1S samples showed slight dimensional deformation of its original shape, a visible slag penetration (Fig. 4) and the presence of macroscopic cracks after the corrosion tests.

On the other hand, the thermodynamic predictions for the IS-6H1S matrix (which contains hydratable alumina as a binder) show that initially a higher amount of spinel and CA_2 can be formed when compared with IS-6C1S (Fig. 3b). These results are related to the higher amount of Al_2O_3 in this system. A significant drop in the liquid slag content in *step 4* was observed due to the formation of CA_2 and spinel. Nevertheless, it must be pointed out that the CaO for the calcium dialuminate formation is only provided by the molten slag. With the advance of the matrix corrosion, CA_6 and corundum were also identified by the simulation results and only 7 steps were required to reach the liquid saturation. Because the resulting liquid from the slag–matrix simulation was saturated in alumina, no reactions between slag and tabular alumina aggregates were detected and, for this reason, the thermodynamic results of this evaluation are not presented here. For the IS-6H1S, the formation of layers around the alumina aggregates was not clearly detected in the castable's microstructure, as for the IS-6C1S samples (Fig. 5). CA_2 was clearly observed at the matrix–slag interface and a mixture of $MgO + MnO + Fe_2O_3$ was also found among the larger grains of spinel and calcium aluminate phases.

Further information that can be inferred by the thermodynamic analysis is related to the changes in the liquid composition, which also can also predict its viscosity at high temperatures. For the IS-6C1S simulations, CaO, Al_2O_3 and SiO_2 contents showed a continuous increase in the liquid phase after each calculation step and the mass balance of these components affected the slag properties at high temperatures. On the other hand, the massive precipitation of CA_2 and CA_6 in

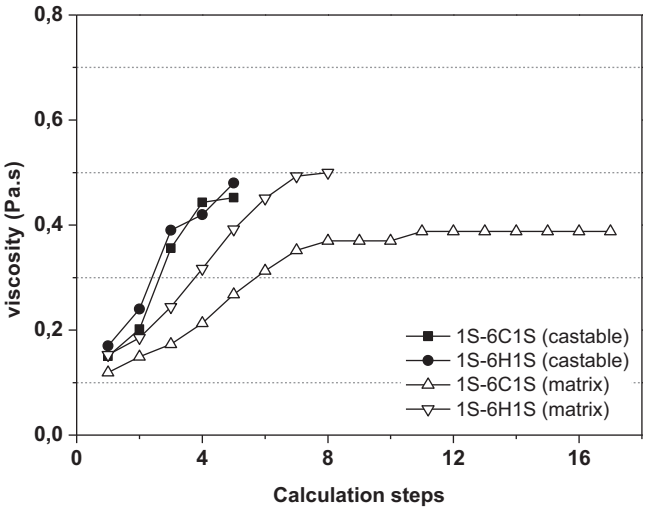

Fig. 6. Thermodynamic predictions of the slag viscosity at 1550 °C.

the IS-6H1S corrosion resulted in a decrease in CaO and Al_2O_3 and higher amounts of SiO_2 were detected in the resulting slag. The estimated viscosity of the resulting liquid attained for each calculation step (simulated using the Viscosity module, FactSage™ – version 6.2, Fig. 6), for the matrix/aggregates or overall castable evaluation, showed the same trend. The higher viscosity of the IS-6H1S liquids is related to the highest amount of SiO_2 in the slag composition and, consequently, the cement free castable should present the lowest slag penetration.

Therefore, based on the thermodynamic predictions, the IS-6H1S should have the highest corrosion resistance because this composition presented a relatively lower liquid content with the highest viscosity and a higher resistance to dissolve alumina.

3.1. Comparison between the thermodynamic simulation models to evaluate castable corrosion behavior

The agreement of various aspects of the corrosion behavior predicted by the thermodynamic simulation shows the usefulness of this tool for supporting experimental results, despite the constraints imposed by the simplifications assumed when the castable overall chemical composition was considered. The same sequence of phase transformations in equilibrium (generation of CA_2, CA_6 and spinel phases at the interface area) during the slag attack of the designed castables was attained for both modeling procedures. However, some improvements were detected when the novel procedure (previous interaction of the liquid slag with the matrix compounds and later with the aggregates) was implemented, i.e., based on the number of calculations required to achieve the liquid saturation, it was possible to clearly identify which composition would be more attacked by the molten slag.

Because the binder source (calcium aluminate cement or hydratable alumina) was the main difference between the two tested compositions, this novel calculation route seems to be the most suitable one. Based on the results presented in Fig. 1, the similarities of the phase contents predicted in the analysis of the overall compositions corrosion behavior should be related to the large amount of tabular alumina aggregates added to the castables, which helped to hide the binder effect on the simulated results.

Spinel and calcium aluminates were detected in the corroded castable samples by the SEM/EDS analyses (Fig. 5) and, the absence of CaO in the IS-6H1S matrix (cement free composition), is most likely the main reason for the absence in its microstructure of CA_2 and CA_6 layers close to the alumina aggregates. This aspect was also confirmed by the calculations shown in Fig. 3 and, after matrix attack, no further corrosion of the tabular alumina was predicted due to the liquid saturation.

4. Conclusions

The tested simulation modeling procedures provided very important information for the understanding of the chemical corrosion behavior of the designed castables. CA_2, CA_6 and $MgAl_2O_{4(ss)}$ were the main phases predicted to be generated after the reaction between molten slag and the refractory. Nevertheless, the limited alumina amount and the presence of calcium aluminate cement as a binder led to a higher slag attack of the IS-6C1S matrix composition (17 calculation steps were required for reaching the liquid saturation). Based on the thermodynamic predictions, the IS-6H1S castable should have the highest corrosion resistance because it presented a relatively lower liquid content with high viscosity and a higher resistance to dissolve alumina. Therefore, the theoretical results are in agreement with the experimental corrosion analysis.

Although the thermodynamic evaluation of the overall composition is able to identify the phase transformation sequence correctly at the interface area between the solid and liquid, a two-step analysis of the liquid contact with the matrix components and later with the aggregate particles seems to be the best alternative to evaluate the differences between the corrosion performance of the two designed refractory materials.

Acknowledgments

The authors are grateful to the Federation for International Refractory Research and Education (FIRE), Magnesita Refratários S.A. (Brazil), FAPESP and CNPq. Additionally, the authors are thankful to the Corus Ceramic Research Centre (CRC) for the microstructure evaluation and corrosion test support.

References

[1] H. Sarpoolaky, S. Zhang, W.E. Lee, Corrosion of high alumina and near stoichiometric spinels in iron-containing silicate slags, J. Eur. Ceram. Soc. 23 (2003) 293–300.
[2] H. Sarpoolaky, S. Zhang, B.B. Argent, W.E. Lee, Influence of grain phase on slag corrosion of low-cement castable refractories, J. Am. Ceram. Soc. 84 (2001) 426–434.
[3] E. Adabifiroozjaei, A. Saidi, A. Monshi, P. Koshy, Effects of different calcium compounds on the corrosion resistance of andalusite-based low-cement castables in contact with molten Al-alloy, Met. Mater. Trans. B 42 (2011) 400–411.
[4] J. Poirier, M.L. Bouchetou, P. Pringent, J. Berjonneau, An overview of refractory corrosion: observations, mechanisms and thermodynamic modeling, Refract. Appl. Trans. 3 (2) (2007) 2–12.
[5] K. Goto, B.B. Argent, W.E. Lee, Corrosion of MgO–$MgAl_2O_4$ spinel refractory bricks by calcium aluminosilicate slag, J. Am. Ceram. Soc. 80 (2) (1997) 461–471.
[6] W.R. Lee, S. Zhang, Melt corrosion of oxides and oxide–carbon refractories, Int. Mater. Rev. 44 (1999) 77–104.
[7] J.P. Guha, Reaction chemistry in dissolution of polycrystalline alumina in lime–alumina–silica slag, Br. Ceram. Trans. 96 (6) (1997) 231–236.
[8] S. Zhang, H.R. Rezaie, H. Sarpoolaky, W.E. Lee, Alumina dissolution into silicate slag, J. Am. Ceram. Soc. 83 (4) (2000) 897–903.
[9] J. Berjonneau, P. Pringent, J. Poirier, The development of a thermodynamic model for Al_2O_3–MgO refractory castable corrosion by secondary metallurgy steel ladle slags, Ceram. Int. 35 (2) (2009) 623–635.
[10] A.P. Luz, A.G. Tomba Martinez, M.A.L. Braulio, V.C. Pandolfelli, Thermodynamic evaluation of spinel containing refractory castables corrosion by secondary metallurgy slag, Ceram. Int. 37 (2011) 1191–1201.
[11] M.D.M. Innocentini, A.R. Studart, R.G. Pileggi, V.C. Pandolfelli, PSD effect on the permeability of refractory castables, Am. Ceram. Soc. Bull. 80 (2001) 31–36.

[12] M.A.L. Braulio, L.R.M. Bittencourt, V.C. Pandolfelli, Selection of binders for in situ spinel refractory castables, J. Eur. Ceram. Soc. 29 (13) (2009) 2727–2735.
[13] M.A.L. Braulio, D.H. Milanez, E.Y. Sako, L.R.M. Bittencourt, V.C. Pandolfelli, Expansion behavior of cement bonded alumina–magnesia refractory castables, Am. Ceram. Soc. Bull. 86 (12) (2007) 9201–9206.
[14] M.A.L. Braulio, A.G. Tomba Martinez, A.P. Luz, C. Liebske, V.C. Pandolfelli, Basic slag attack of spinel-containing refractory castables, Ceramics International 37 (2011) 1935–1945.
[15] S. Yilmaz, Corrosion of high alumina spinel castables by steel ladle slag, Ironmak. Steelmak. 33 (2) (2006) 151–156.